Computers and Chemical Engineering 210 (2026) 109633

Contents lists available at ScienceDirect

Computers and Chemical Engineering

journal homepage: www.elsevier.com/locate/compchemeng

Modeling VOC emissions from hydrocarbon tanks: mechanistic insights vs. inventory approaches

Diego Rampi, Francesca Tagliaferri, Marzio Invernizzi *

Politecnico di Milano, Department of Chemistry, Materials and Chemical Engineering "Giulio Natta" - P.za Leonardo da Vinci 32, 20133 Milano, Italy

ARTICLE INFO

Dataset link: Numerical model implementation and simulation code for VOC tank emission modeling (Original data)

Keywords:
Modeling
Inventory
Emissions
Comparison
Storage tanks

ABSTRACT

Volatile Organic Compounds (VOCs) released from storage tanks represent a major source of air pollutants in refineries and petrochemical facilities. This study benchmarks the phenomenological tank–headspace model of Rota et al. (2001) against the standard US EPA's AP-42 methodology using one year of hourly operational data from diesel tanks. The former formulation was re-implemented through numerical stabilization with flux limiters and a condensation sub-model, improving robustness under steep gradients and enabling to capture the possible vapor recondensation absent from the original scheme. Both approaches reproduce seasonal emission cycles but diverge in their ability to resolve transient events: the mechanistic model captures filling/emptying peaks and headspace dynamics, while AP-42 remains primarily temperature-driven. Annual emission totals are comparable, with AP-42 offering a rapid, low-input solution for inventories, and Rota et al. (2001) providing enhanced temporal resolution for short-term exposure. Results highlight a trade-off between computational demand and temporal resolution, with implications for regulatory versus process-level applications.

1. Introduction

Volatile Organic Compounds (VOCs) comprise a diverse group of carbon-based substances that evaporate at ambient temperatures and may be dispersed into the atmosphere, where they exert significant influence on both environmental processes and public health (Duan et al., 2023; Mellouki et al., 2015).

VOCs act as major precursors of ground-level ozone and secondary organic aerosols (SOA), two key drivers of deteriorating air quality in urban and industrial regions (Pandey and Yadav, 2018; Zhou et al., 2023). Under sunlight and in the presence of nitrogen oxides (NO_x), VOCs initiate radical-based oxidation cycles that catalyze ozone production (Atkinson, 1990; Kansal, 2009; Mellouki et al., 2015). The SOAs produced through VOC oxidation, in turn, represent a critical fraction of fine particulate matter (PM2.5), with broad impacts on visibility, cloud microphysics, and climate regulation (Bo et al., 2008; Wei et al., 2022). The formation, transformation, and spatial dispersion of ozone and SOAs are strongly modulated by local meteorology, emission patterns, and VOC chemical composition (Bo et al., 2008; Guenther, 1997).

Beyond their atmospheric reactivity, many VOCs such as benzene, toluene, and formaldehyde, are directly toxic or carcinogenic, linked to neurological disorders, hematological diseases, and chronic respiratory conditions. Beyond these direct risks, indirect health impacts arise from elevated ozone and PM2.5, which drive widespread respiratory and cardiovascular disease (Soni et al., 2018; Wei et al., 2022; Zhou et al., 2025, 2023). At the ecosystem level, VOC-driven processes reduce crop yields, impair photosynthesis, and accelerate biodiversity loss, while also amplifying vulnerability to pathogens and pests through oxidative stress (Dicke et al., 2010; Dicke and Baldwin, 2010; Holopainen and Gershenzon, 2010; Kegge and Pierik, 2010). Additionally, VOC emissions can intensify environmental stressors such as soil acidification and nutrient loading, further complicating ecosystem health management. Consequently, effective regulation of VOC emissions is essential to safeguard air quality and protect both public health and the environment (Duan et al., 2023; Fetisov et al., 2023; Pandey and Yadav, 2018; Zhou et al., 2023).

The chemical structures of VOCs range from simple hydrocarbons (e.g., alkanes, olefins) to more complex aromatic and oxygenated compounds (e.g., aldehydes, ketones, esters) (Duan et al., 2023; Pandey and Yadav, 2018; Zhou et al., 2023). This intrinsic diversity leads to considerable differences in reactivity and atmospheric lifetime, making VOC emission management particularly challenging (Atkinson, 1990; Duan et al., 2023; Kansal, 2009; Mellouki et al., 2015). Nevertheless, extensive research confirms that VOCs play a critical role in air quality issues, directly impacting ecosystems, climate, and human health (Duan

* Corresponding author.
E-mail address: marzio.invernizzi@polimi.it (M. Invernizzi).

https://doi.org/10.1016/j.compchemeng.2026.109633
Received 13 October 2025; Received in revised form 20 February 2026; Accepted 10 March 2026
Available online 11 March 2026

et al., 2023; Soni et al., 2018; Zhou et al., 2025, 2023).

Despite substantial progress in chemical characterization, atmospheric dispersion, and assessment of health impacts, the diversity of emission sources, VOC regulation still faces significant gaps. These primarily arise due to the heterogeneity of VOC species, the diversity of emission sources, and the highly dynamic nature of atmospheric processes (Bo et al., 2008; Kansal, 2009; Piccot et al., 1992). In addition, emissions arise from shifting mixes of biogenic species that dominate globally and anthropogenic outputs that prevail in urban or industrial hotspots (Liaskoni et al., 2024; Niinemets, 2010; Xing et al., 2024). Accurate quantification of these fluxes requires advanced chromatographic or optical techniques; nevertheless, emission inventories often underrepresent key species or temporal variability (Chen et al., 2022; Invernizzi et al., 2025, 2021). Meteorological conditions and radical chemistry compress or extend lifetimes, reshaping local risk profiles (Bo et al., 2008; Kansal, 2009; Sun et al., 2025). Furthermore, as temperature, sunlight and industrial activity fluctuate throughout the day, the relative contribution of each source varies from hour to hour (Tagliaferri et al., 2023). This moving target complicates emission inventories and the design of effective policies (Pandey and Yadav, 2018).

With advances in modeling and measurement techniques, research has increasingly focused on VOC sources notably influencing local and regional pollution episodes (Polvara et al., 2021; Wang et al., 2013). Among these, hydrocarbon storage facilities represent significant emission sources, generating short-term, high-concentration plumes that can lead to ozone exceedances and odor nuisance episodes (Invernizzi and Sironi, 2021; Rota et al., 2001; Tagliaferri et al., 2026).

Refineries and petrochemicals rank among the largest anthropogenic VOC sources; emissions arise from process units, leaks, flares, wastewater, maintenance, and—critically—product storage and transfer (Polvara et al., 2021; Wang et al., 2013). Storage tanks are especially important because their large surface area and variable operating conditions may favour evaporation (Batić, 2023; Invernizzi et al., 2021; Sun et al., 2025). The emission mechanism is constituted by two main contributions:

- Standing (*breathing*) losses: diurnal and barometric oscillations expand or contract the vapour space, venting VOC-laden air even when tanks sit idle (Moncalvo et al., 2016).
- Working losses: each filling or emptying operation displaces headspace gas through the vents; during refilling, the incoming air is rapidly brought toward saturation, so the displaced volume yields short-term emissions that scale with throughput and saturation factors (Rota et al., 2001; Saikomol et al., 2019).

The state of the art for the quantification of the VOC emissions from storage tanks relies on semi-empirical correlations (Pascal et al., 2015). These algorithms are based on a specific methodology and are described in the U.S. EPA's AP-42 Chapter 7 (U.S. Environmental Protection Agency, 2020). Recently, the US EPA has also released an updated version of the TANKS software, which incorporates the AP-42 Chapter 7 correlations, able to estimate breathing and working losses by combining tank geometry, local meteorology and fluid thermodynamics, yielding monthly or annual averages that satisfy inventory requirements (U.S. Environmental Protection Agency, 2020). However, the coarse temporal resolution and simplifying assumptions—i.e. uniform vapour space—can underpredict short-term peaks caused by stratified temperatures, blend switches or clustered filling operations and lose accuracy for multicomponent streams or partially insulated, non-canonical tanks (Invernizzi et al., 2021; Moncalvo et al., 2016; Wang et al., 2018). To address these limitations, phenomenological models have been developed that explicitly solve the coupled unsteady mass- and energy-balance equations governing heat transfer, phase equilibrium and vapour transport within the vessel, thus capturing solar loading, ambient fluctuations and operational transients. Preliminary simulations show, for instance, that a mid-day summer filling operation can emit several-fold more VOC than an otherwise identical night-time transfer—insight vital for exposure assessment and schedule optimisation (Moncalvo et al., 2016; Zinke et al., 2020).

The objective of this study is to benchmark an advanced tank-breathing model against the simplified methodology prescribed by the U.S. EPA AP-42. The full transient mass- and energy-balance formulation originally proposed by Rota et al. (2001) was re-implemented and customised to the operating profile of four real-case fixed-roof diesel tanks, for which hourly measurement of liquid level, product temperature and ambient temperature were available for an entire year. Two key enhancements were introduced to strengthen the model usability: (i) total-variation-diminishing flux limiters (LeVeque, 1990; Sweby, 1984), to stabilise the numerical scheme across sharp thermal and concentration gradients, and (ii) a condensation sub-model that can account for partial vapour recondensation along the upward path, thereby capturing a potential phenomenon absent from the original formulations.

The comparison with the AP-42 semi-empirical correlations is intended as a structured benchmarking against the prevailing regulatory framework rather than as a validation against an experimental reference. AP-42 is therefore adopted as a widely used and standardized inventory methodology that provides a practical baseline for interpreting differences in model structure, temporal resolution, and response to operational variability.

The refined solver is so evaluated against the AP-42 semi-empirical correlations (U.S. Environmental Protection Agency, 2020) in terms of (a) its behaviour in reproducing vent-stream concentrations and total VOC mass flux, and (b) the predictive variations obtained relative to the substantial increase in computational cost and model complexity.

Accordingly, the contribution of this work lies in the comparative assessment of modeling philosophies, i.e. transient-resolving mechanistic simulation versus semi-empirical inventory formulation, under realistic refinery operating conditions, rather than in independent experimental validation.

This work systematically compares a refined tank-breathing model with standard inventory methodologies. It also introduces targeted modifications to the advanced model to enhance its numerical stability and, prospectively, predictive capability.

2. Materials and methods

To overcome the approximations inherent in traditional methodologies, the phenomenological model developed by Rota et al. (2001) captures the vertical and temporal gradients of temperature and vapour composition inside the gaseous headspace of a fixed-roof tank, solving coupled mass- and energy-balance equations that unify standing and working losses within one framework (Rota et al., 2001).

A key output of this model is the instantaneous vapour-phase concentration at the roof vent, C_{top}, which in the present study is compared with the working-loss vapour factor W_v specified in the AP-42 guidance (U.S. Environmental Protection Agency, 2020). By updating the post-cycle vapour state as the initial condition for the next operating step, the model can quantify cumulative heat- and mass-build-up effects over time. This state-dependent evolution enables the assessment of alternative loading schedules and abrupt environmental changes that cannot be captured by semi-empirical, quasi-steady inventory correlations.

2.1. State of the art: AP-42 correlations

In the US EPA AP-42 framework, the stock-vapour density is expressed as:

$$W_v = \frac{M_v P_{vA}}{R T_V} \tag{1}$$

$$P_{vA} = \exp\left[A - \frac{B}{T_{LA}}\right] \tag{2}$$

Where M_v is the molecular weight of the equilibrium vapour, R the gas constant, A,B the Antoine coefficients of the stored liquid, and the two characteristic temperatures are defined empirically rather than through a detailed heat-balance. For long-term average estimates, Chapter 7 (U. S. Environmental Protection Agency, 2020) offers the present shortcuts:

$$T_{LA} = 0.3T_{AA} + 0.7T_B + 0.005\alpha_R I \tag{3}$$

$$T_V = 0.7T_{AA} + 0.3T_B + 0.009\alpha_R I \tag{4}$$

With:

T_{LA} = average liquid surface temperature [°R]
T_V = average vapour-space temperature [°R]
T_{AA} = annual-average ambient temperature [°R]
T_B = average bulk-liquid temperature [°R]
α_R = solar absorptance of the tank's paint [-]
I = annual-average insolation [Btu/ft^2/d]

Eqs. (3) and (4) incorporate the effects of solar loading and paint colour through the linear $\alpha_R I$ term and weight the influence of ambient and bulk temperatures differently for liquid and vapour phases (70 % vs 30 % in each case). Using these empirical correlations removes the need for detailed diurnal heat-balance calculations while still capturing first-order radiative effects. The vapour density W_V obtained from Eq. (1) is thus the composition-dependent metric against which the roof-vent concentration C_{top}, predicted by the Rota et al. (2001), model will be compared.

2.2. Phenomenological model: equations, boundary conditions and correlations

In the original work presented by Rota et al. (2001), two fundamental equations are introduced to describe the behavior of the gas (air-hydrocarbon mixture) inside a fixed-roof tank, assuming that the dynamics are predominantly one-dimensional along the vertical direction (y-axis).

To simplify the treatment of a moving interface during tank filling and emptying cycles, the spatial coordinate along the vertical axis of the tank is non-dimensionalized, defining:

$$y = \frac{z}{H(t)} \tag{5}$$

where z is the physical vertical coordinate [m], and $H(t)$ is the instantaneous vapor-space height, which varies over time due to the inflow and outflow of liquid. This transformation maps the physical domain $z \in [0, H(t)]$ into a fixed computational domain $y \in [0,1]$, thereby eliminating the need to remesh the domain dynamically.

This approach greatly simplifies the numerical implementation by allowing the use of fixed boundary conditions and a constant spatial discretization, despite the physical height of the vapor phase varying over time. In essence, the coordinate transformation transforms a moving-boundary problem into one with static boundaries, without loss of generality in capturing dynamic tank behaviour.

The basic model equations consist of two coupled PDEs for temperature and concentration in the vapor phase:

$$\begin{cases} \dfrac{\delta T}{\delta t} - \dfrac{y\bar{v} + (v^* - \bar{v})}{\bar{v}t - H}\dfrac{\delta T}{\delta y} - \dfrac{\alpha}{T_{ILG}(\bar{v}t - H)^2}\left(T\dfrac{\delta^2 T}{\delta y^2} - \left(\dfrac{\delta T}{\delta y}\right)^2 + \dfrac{\delta T}{\delta y}\dfrac{\delta T}{\delta y}\Big|_{y=0}\right) = 0 \\ \dfrac{\delta C}{\delta t} - \dfrac{y\bar{v} + (v^* - \bar{v})}{\bar{v}t - H}\dfrac{\delta C}{\delta y} - \dfrac{E}{(\bar{v}t - H)^2}\dfrac{\delta^2 C}{\delta y^2} + \dfrac{\alpha}{T_{ILG}(\bar{v}t - H)^2}\left(\dfrac{\delta C}{\delta y}\left(\dfrac{\delta T}{\delta y} - \dfrac{\delta T}{\delta y}\Big|_{y=0}\right) + C\dfrac{\delta^2 T}{\delta y^2}\right) = 0 \end{cases} \tag{6}$$

Where:

C = vapor-phase hydrocarbon concentration [kmol/m^3]
T = vapor-phase temperature [K]
$\bar{v}$ = interface displacement velocity (liquid level movement) [m/s]
v^* = net liquid-to-gas transport velocity [m/s]
H = tank height [m]
$\alpha = \frac{ET}{\rho_{ILG} C_P}$ [-]
E = axial mass dispersion coefficient [m^2/s]
E_T = axial thermal dispersion coefficient [m^2/s]
T_{ILG} = liquid-gas interface temperature [K]
T_t = roof temperature [K]

The coefficients E and E_T were calculated based on correlations involving the material and thermal Peclet numbers, as reported in Butt (2000).

The boundary conditions of Eq. (6) are:

$$T|_{y=0} = T_{ILG} \tag{7}$$

$$T|_{y=1} = T_t \tag{8}$$

$$C|_{y=0} = C_{sat}(T_{ILG}) \tag{9}$$

$$\begin{cases} \dfrac{\delta C}{\delta y}\Big|_{y=1;v(y=1)>0} = 0 \ \textit{exhale} \\ E\dfrac{\delta C}{\delta y}\Big|_{y=1;v(y=1)<0} = (Cv)|_{y=1}(H - \bar{v}t) \ \textit{inhale} \end{cases} \tag{10}$$

Where T_{ILG} is calculated through a pseudo-steady-state energy balance at the liquid–gas interface, and C_{sat} is determined using an appropriate Antoine equation.

2.3. Structure of the simulation code and role of the flux limiters

The simulation code was developed in MATLAB 2024a using a simplified 1D finite-difference approach to solve the governing partial differential equations (PDEs) describing mass and energy transport in the vapor phase of the tank. Simulations were run on an HP 255 G8 Notebook PC (AMD Ryzen 3 3250 U, 2 cores / 4 threads, up to 3.5 GHz; 8 GB RAM; NVMe SSD; Windows 11; MATLAB R2024a, no GPU/parallel).

The computational structure is modular and divided into the following key components:

2.3.1. Parameter definitions

All relevant thermophysical properties (e.g., vapor pressure, molar mass, heat capacities, viscosity, diffusivity, Antoine constants), as well as tank dimensions and operating conditions, are grouped within a structured variable `params`. This design enables flexible changes and modular access to physical constants and simulation settings.

2.3.2. Spatial discretization

The normalized vertical coordinate $y \in [0,1]$ is discretized into N nodes with uniform spacing $\Delta y = 1/N$. The discretization transforms the original PDE system into a set of coupled ordinary differential equations

(ODEs) for temperature and concentration at each node.

The selected spatial grid density and adaptive solver tolerances were chosen as a compromise between numerical stability and computational efficiency, ensuring converged and robust solutions without altering the physical response of the system; additional simulations with refined grids and stricter tolerances confirmed negligible variations in transient peak magnitudes and cumulative emissions.

The first derivatives (convective terms) are approximated using finite differences, corrected by flux limiter functions ϕ (LeVeque, 1990; Sweby, 1984) to avoid numerical instabilities near steep gradients or discontinuities:

$$\left(\frac{\delta C}{\delta y}\right)_i = \phi(r_i)\frac{C_{i+1} - C_i}{\Delta y} \tag{11}$$

where:

$$r_i = \frac{C_i - C_{i-1}}{C_{i+1} - C_i} \tag{12}$$

The second derivatives (diffusive terms) are computed using classic centered schemes:

$$\left(\frac{\delta^2 C}{\delta y^2}\right)_i = \frac{C_{i+1} - 2C_i + C_{i-1}}{\Delta y^2} \tag{13}$$

Analogous formulations are used for the temperature derivatives discretization; the resulting ODE system has dimension $2N$, accounting for one equation per node for both concentration and temperature.

The selected spatial discretization and solver tolerance settings were chosen as a compromise between numerical stability and computational efficiency, ensuring convergence and robustness without altering the physical response of the system.

2.3.3. Numerical modifications of boundary conditions

In the original formulation by Rota et al. (2001), boundary conditions at the tank roof for vapor concentration are presented as two distinct differential relations, depending on whether the vapor velocity $\bar{v}$ is directed outward ($\bar{v} > 0$) or inward ($\bar{v} < 0$). However, direct implementation of these differential boundary conditions led to numerical difficulties related to the resulting Differential-Algebraic Equation (DAE) system having an index greater than one, which posed computational challenges.

To overcome this, the boundary conditions were converted from differential to algebraic form. Specifically, when $\bar{v} > 0$, a straightforward algebraic approximation was adopted, imposing a zero-gradient condition at the roof, i.e. the vapor concentration at the top node (N) equals that of the node immediately below ($N - 1$):

$$C|_N = C|_{N-1} \tag{14}$$

Conversely, the boundary condition for the case $\bar{v} < 0$, originally dependent on the axial dispersion coefficient E, itself linked implicitly to the solution, could not be easily algebraically transformed. After multiple trials with alternative approaches, a simplified yet physically consistent modification was introduced, effectively capturing the phenomenon of vapor dilution due to air inflow:

$$C|_N = C|_{N-1} \cdot \frac{V_{up}}{V_{up} + \bar{v} \cdot \frac{\pi D_{TK}^2}{4}} \tag{15}$$

In these expressions, N denotes the total number of discretization nodes along the vertical computational grid; consequently, the index N corresponds to the uppermost node, representing the vapor-phase concentration at the tank roof, while $N - 1$ is the immediately adjacent node below. This algebraic boundary condition accounts explicitly for vapor inflow dilution by considering the instantaneous vapor-space volume (V_{up}) and inward flux ($\bar{v} \cdot \frac{\pi D_{TK}^2}{4}$), where D_{TK} is the tank's diameter, thus ensuring computational robustness without significantly compromising the predicted concentration dynamics.

2.3.4. Flux limiters

The convective terms are handled using a limited high-resolution scheme, designed to blend between first-order upwind (monotonic but diffusive) and second-order central (accurate but oscillatory) schemes. This is achieved using a flux limiter function $\phi(r)$, where r is the ratio of successive solution gradients (LeVeque, 1990; Sweby, 1984).

Several limiter types are implemented in the code:

- Minmod: $\phi(r) = \max(0, \min(1, r))$
- Superbee: $\phi(r) = \max(0, \min(2r, 1), \min(r, 2))$
- Van Leer: $\phi(r) = \frac{r + |r|}{1 + |r|}$

These limiters are applied point-by-point along the spatial grid to modulate the anti-diffusive flux, allowing the model to resolve non-smooth phenomena such as sharp vapor concentration gradients near the liquid interface, while avoiding spurious oscillations common in pure second-order schemes.

In the present work, flux limiting was introduced as a numerical stabilization mechanism rather than as a modification of the underlying physical model. The limiter acts solely on the convective flux reconstruction to ensure boundedness and monotonicity of the numerical solution, while preserving the consistency of the discretized equations.

Preliminary comparative simulations conducted over shorter time intervals showed that the limiter effectively suppresses non-physical oscillations and concentration overshoots near steep gradients, while preserving the overall transient solution behaviour. In contrast, simulations without flux limiting exhibited progressively growing numerical instabilities under stiff transient conditions, ultimately compromising convergence in extended (year-long) runs. After preliminary evaluations, for the simulations carried out in this study the Superbee limiter emerged as the most efficient; this finding reflects case-specific numerical performance rather than a general conclusion from the literature.

2.3.5. Time integration with ode15s

The semi-discretized ODE system was solved using MATLAB's stiff solver ode15s, chosen for its robustness in handling stiff problems typical of thermal-diffusive systems. The solver integrates over time windows corresponding to filling, idle, and emptying phases, allowing for dynamic boundary conditions.

2.3.6. Filling/Emptying cycle management

The function $\bar{v}(t)$ (average interface velocity) is defined piecewise over each cycle: filling (positive velocity), idle (zero), and emptying (negative velocity). This time-varying function is updated at each time step and used in the convection terms of the PDE system to reflect the real operating behaviour of the tank.

2.4. Code implementation and reproduction of published benchmark cases

To test the developed code and evaluate its consistency with the original model by Rota et al. (2001), two modeling tests, originally reported in Rota et al. (2001), were replicated. The first test corresponds to a laboratory-scale experiment reported in Fig. 3 of the cited manuscript, using heptane as the stored liquid. The second test refers to the industrial-scale experiment presented in Fig. 5 of the same work.

In both cases, to enable a more direct and meaningful comparison between the phenomenological model and the AP-42 method, the temperatures used in the original work of Rota et al. (2001), namely the vapor-liquid interface temperature (T_{ILG}) and the internal roof temperature (T_t), were replaced with the temperatures calculated using the AP-42 methodology: the liquid-surface temperature (T_{LA}) and the vapor temperature (T_V) from Eq. (3) and (4).

The main parameters of the two experiments are summarized below:

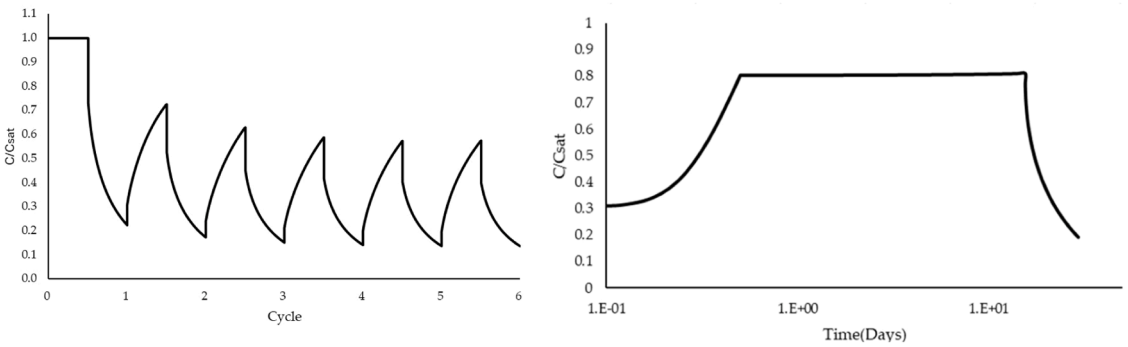

Fig. 1. Replication of the laboratory-scale test (left) and the industrial-scale test (right) obtained with the developed code. The corresponding original results are reported in Figs. 3 and 5 of Rota et al. (2001), respectively.

- **Laboratory-scale experiment**: A vertical plastic column with a height of 3.1 m and an internal diameter of 0.075 m was used. The liquid level was cyclically varied, leading to transient changes in vapor composition at the tank top, measured over multiple cycles until a periodic steady state was achieved (Fig. 1, left).
- **Industrial-scale experiment**: Real-scale storage tanks with a capacity of approximately 3500 m^3 and a height of 14 m, insulated with rock wool, were used to monitor emissions of acetic acid under actual operating conditions, including filling, standing, and emptying stages (Fig. 1, right).

The results from Rota et al. (2001) are presented in terms of the ratio C/C_{sat}, where C is the concentration calculated by the PDE system at the roof (last spatial node) and C_{sat} is the saturation concentration at the liquid-gas interface. The replicated simulations, using AP-42 temperatures, reproduced these results with negligible discrepancies. Notably, minor differences may arise due to incomplete information on key physical properties, such as diffusivity, which may significantly affect model behaviour. Additionally, the use of flux limiters, introduced to better handle sharp gradients or points of non-differentiability in the numerical solution, may have also contributed to slight variations compared to the original results.

The close agreement between the present implementation and the results reported by Rota et al. (2001) indicates that the algebraic reformulation of the roof boundary condition does not introduce systematic bias in the predicted vapor concentrations. This confirms that the modified boundary condition preserves the physical behaviour of the original model while improving the numerical stability of the discretized system.

Therefore, the internal consistency of the numerical implementation and its faithful reproduction of the dynamic behaviour reported by Rota et al. (2001) confirm the robustness of the proposed formulation; for the original figures replicated in this work, the reader is referred to Rota et al. (2001).

2.5. Adaptation of the original model with real diesel data

In the second phase of the study, the original code was extended with year-long operational data from a real industrial case study. The dataset included measurements of the liquid level inside the tanks, which allowed for the calculation of the hourly average vapor velocity ($\bar{v}$), and measurements of the liquid temperature, which, as previously mentioned, was used to calculate T_{LA} with Eq. (3) (assumed to be equal to the vapor-liquid interface temperature T_{ILG}). The data used in this study were obtained, on an hourly basis, from the Distributed Control System (DCS) of the industrial complex. In addition, measurements of the ambient temperature T_{AA} near the tanks (3 km far away) were used to calculate the internal roof temperature with Eq. (4). As regards the thermodynamic and chemical-physical data of diesel, an extended table with numerical values and sources is provided (a representative temperature of 25 °C was chosen so that property values could be treated as constant, following (Ra et al., 2009), thereby simplifying the calculations) (Table 1).

Table 1
Thermodynamic and physicochemical properties of diesel adopted in the simulations.

Variable symbol	Variable name	Value	u.o.m	References & Notes
M_W	Molecular weight	0.13	kg/mol	(U.S. Environmental Protection Agency, 2020)
k_G	Gas-phase thermal conductivity	$2.5 \bullet 10^{-2}$	W/m/K	Hypothesized constant and equals to k_{AIR}
D	Liquid-gas diffusivity	10^{-5}	m^2/s	Hypothesized constant (Elliott~ and Watts, n.d.)
k_L	Liquid-phase thermal conductivity	0.14	W/m/K	Hypothesized constant (Ra et al., 2009)
μ_L	Dynamic viscosity	$2 \bullet 10^{-3}$	N•s/m^2	Hypothesized constant (Ra et al., 2009)
c_{pL}	Specific heat capacity	2050	J/kg/K	Hypothesized constant (Ra et al., 2009)
ρ_L	Liquid density	835	kg/m^3	Hypothesized constant (U.S. Environmental Protection Agency, 2020)
ΔH_{vap}	Latent heat of evaporation	46,800	J/mol	Hypothesized constant (Ra et al., 2009)

Emissions were simulated over the full annual cycle, and the resulting data were analysed by plotting the ratio C/C_{sat}, which enabled a more detailed investigation of system behaviour. In this case, C_{sat} was calculated at the same spatial point as C, specifically at the last node of the computational domain — the point where vapor emissions occur, namely, according to Rota et al. (2001), C_{top}. Interestingly, it was observed that in several periods of the year, the C/C_{sat} ratio exceeded unity, indicating supersaturation conditions at the emission point.

This finding revealed a potential limitation of the original model, namely, the absence of a mechanism to account for vapor condensation. In the absence of such a treatment, the model may fail to reproduce situations where the vapor phase locally exceeds the saturation limit, which is physically unrealistic. To address this issue, the model was extended by introducing a saturation-based correction aimed at constraining vapor concentration to thermodynamic equilibrium conditions and accounting, in a simplified manner, for the effects of condensation on emission behaviour (Fig. 2).

2.6. Model extension to include vapor condensation effects

To address the limitation identified in the original models — namely, the occurrence of local vapor concentrations exceeding the saturation

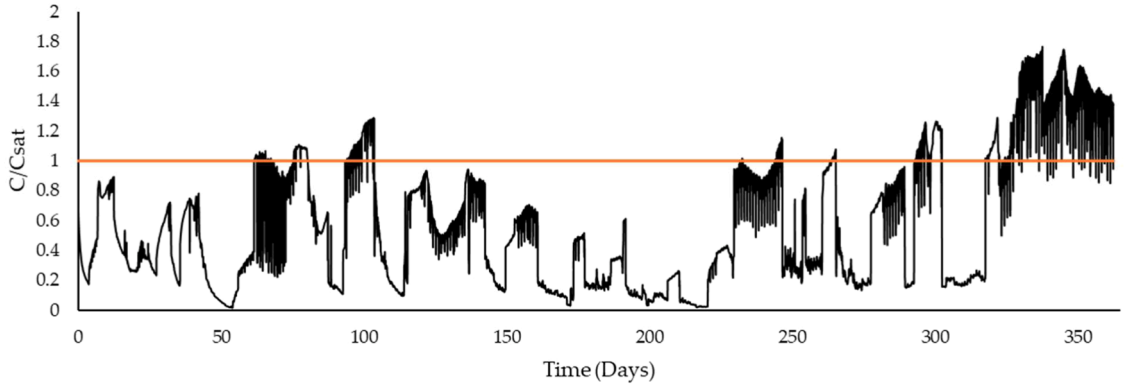

Fig. 2. Temporal profile of C/C_{sat} ratio at the emission point without accounting for vapor condensation.

value — a correction method was introduced. During each time step and at every spatial node, the vapor concentration C_{calc} computed by the transport equations was compared to the corresponding local saturation concentration C_{sat}. The corrected concentration was then defined as:

$$C = min\ (C_{calc}, C_{sat}) \tag{16}$$

This procedure ensures that, at any point within the computational domain, the vapor concentration cannot exceed the saturation limit, thus maintaining the physical consistency of the model under all operating conditions. Fig. 3 presents the time evolution of C/C_{sat} obtained with the condensation correction.

Rather than applying a saturation constraint solely at the emission point (i.e., the last spatial node), the correction was implemented across the entire vapor space. This choice provides a more physically consistent representation of the vapor phase behaviour without resorting to a significantly more complex modeling framework.

A full treatment of condensation phenomena would require the explicit description of droplet nucleation and growth during vapor ascent, involving the introduction of additional mass and energy balances over a two-phase control volume (Majumdar et al., 2023). Such an approach, although more rigorous, would substantially increase the model complexity and computational burden, making it impractical for the intended long-term, real-data-based simulations.

Specifically, a fully coupled formulation would require additional state variables to track condensate mass, latent heat release, interfacial transport processes, effective condensation areas and phase-transfer coefficients at tank scale. Many of these quantities are not directly measurable under real operating conditions and would introduce additional uncertainty without proportionate benefits for the long-term emission assessment targeted in this study.

The adopted correction strategy represents a pragmatic compromise: it allows for the physical phenomenon of condensation to be accounted for in a simplified manner, preserving both the interpretability and computational efficiency of the model.

From a numerical standpoint, enforcing the condition $C = min\ (C_{calc}, C_{sat})$ also significantly enhances the stability and robustness of the solution algorithm. By preventing the occurrence of unphysical supersaturation and the associated steep concentration gradients, the method reduces the risk of numerical oscillations or artifacts, particularly in regions where strong vapor-phase stratification occurs. This is especially beneficial when using flux limiters or high-resolution numerical schemes, which are designed to accurately capture steep gradients while minimizing numerical diffusion.

To summarise, the proposed condensation treatment does not constitute a fully coupled two-phase mass and energy balance with explicit droplet dynamics; rather, it introduces a thermodynamically consistent phase-equilibrium constraint that prevents non-physical supersaturation while preserving numerical stability and computational tractability.

3. Results

3.1. Case-study description

The investigated case study is a refinery located in Southern Italy, positioned near the coastal interface between land and sea. The analysis focuses on four welded fixed-roof diesel storage tanks, designated TK_A, TK_B, TK_C, and TK_D.

Diesel was selected as the reference product because it represents one of the most widely produced, stored, and transferred oil&gas streams worldwide in fixed-roof diesel tanks. These items typically operate at large capacities and constitute a significant and persistent source category in refinery VOC inventories, making them a relevant and representative case for evaluating emission modelling approaches.

Each tank is equipped with a cone-shaped roof and has standard dimensions: approximately 18 m in height and 50 m in diameter.

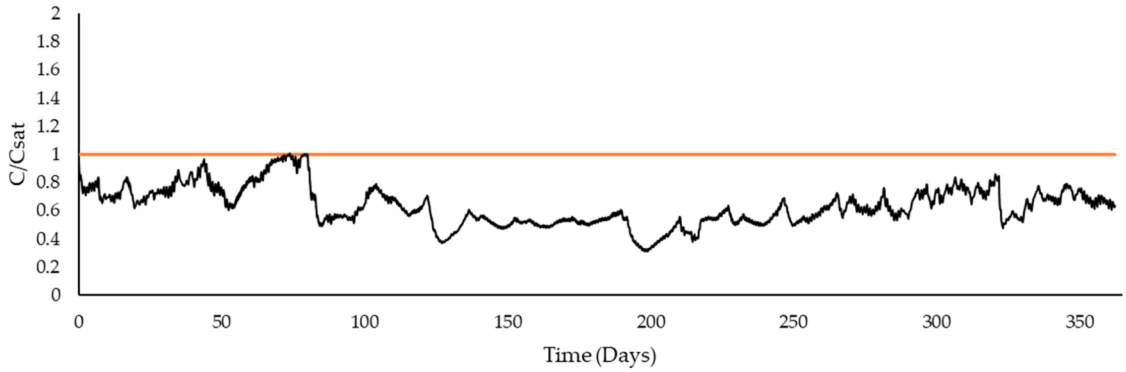

Fig. 3. Temporal profile of C/C_{sat} ratio at the emission point after implementing the condensation correction.

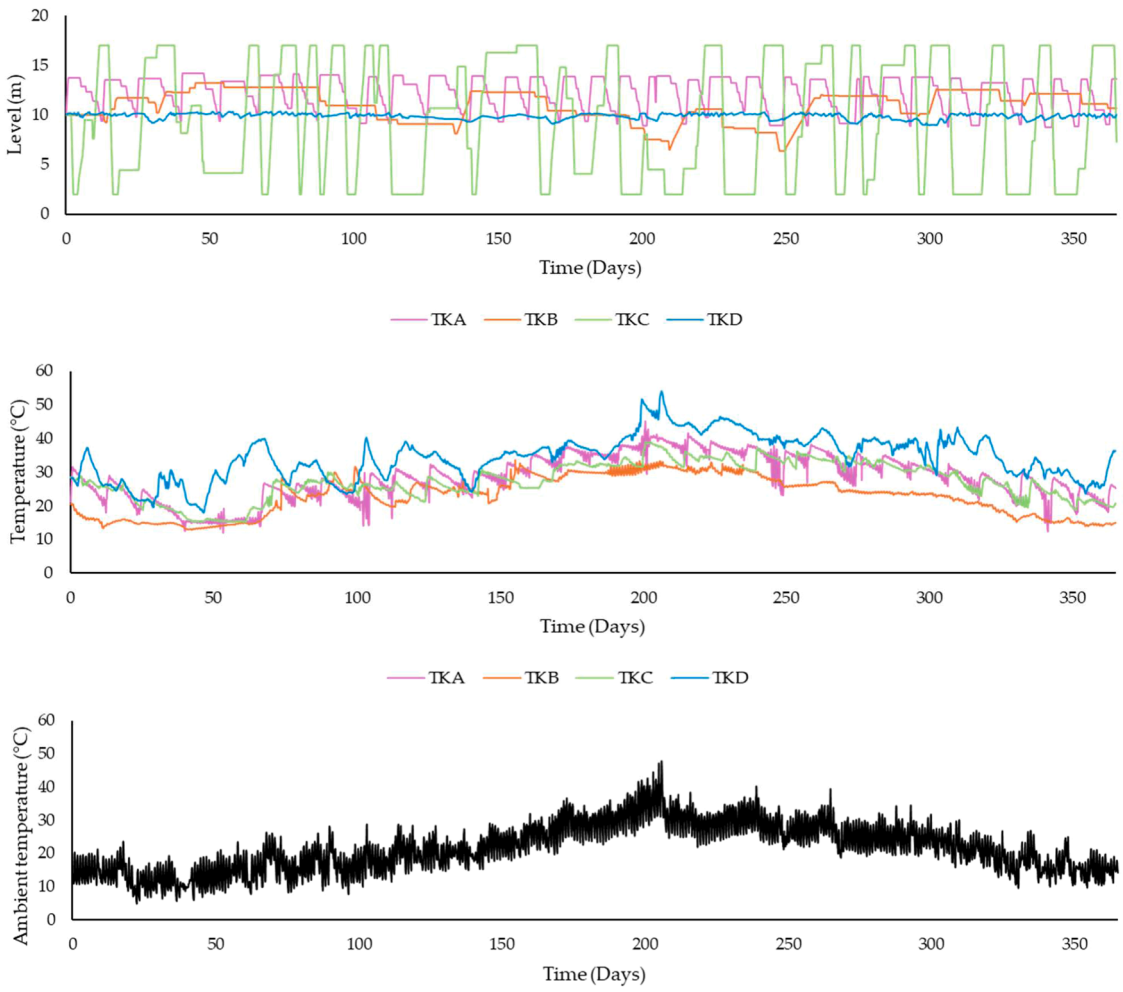

Fig. 4. Annual profile of hourly liquid level variations in the tanks (a), hourly liquid level variations in the tanks (b), hourly ambient air temperatures measured at the refinery site (c).

Operational data for one year were collected from the refinery's DCS, which provided hourly measurements of liquid levels and bulk-liquid temperatures (T_B). Ambient air temperatures (T_{AA}) were recorded separately by the local weather station. These datasets served as boundary conditions and inputs for the numerical models. The detailed operational profiles of the tanks are presented in Fig. 4.

Fig. 4 provides a clear rationale for the selection of these four tanks, demonstrating their substantially different operating patterns. Specifically, TK_C and TK_D exhibit nearly opposite operational behaviours: TK_C undergoes significant and frequent fluctuations, with liquid levels varying dramatically between approximately 2 m and 17 m, while TK_D remains almost constant throughout the year, at about 10 m. TK_A and TK_B represent intermediate operational behaviours, with levels ranging from approximately 7 m to 14 m, differing primarily in the nature of their filling cycles—TK_A features rapid and highly oscillatory cycles, whereas TK_B is characterized by smoother and more gradual filling and emptying cycles.

3.2. *Comparative evaluation of AP-42, Rota et al. (2001) and condensation models*

A comprehensive comparison between the different modeling approaches is presented for each tank (TK_A, TK_B, TK_C, TK_D).

The considered approaches include:

1. The phenomenological model by Rota et al. (2001).
2. The phenomenological model by Rota et al. (2001), modified to account explicitly for condensation effects.
3. The standard AP-42 method (U.S. Environmental Protection Agency, 2020).
4. A modified AP-42 method incorporating a simplified condensation correction. This modification consists of calculating vapor pressure P_{VA} using the minimum temperature between the vapor temperature T_V and the liquid-surface temperature T_{LA} (Eq. (2)–(4)).

For each tank, the comparisons are presented in three graphs (Fig. 5), with each plot showing the vapor densities at the tank roof (expressed in g/m^3) throughout the year:

- Graph (a): AP-42 (U.S. Environmental Protection Agency, 2020) (standard) vs. Rota et al. (2001) (standard).
- Graph (b): Rota et al. (2001) (standard) vs. Rota et al. (2001) (modified with condensation).
- Graph (c): AP-42 (U.S. Environmental Protection Agency, 2020) (modified with condensation) vs. Rota et al. (2001) (modified with condensation).

In order to assess how the different may impact on the emission inventory, annual emissions were calculated: these data have been obatinedby summing the emitted mass over all hourly time steps throughout the year. For each time step, the emitted mass was obtained by multiplying the vapor-phase concentration predicted at the roof node by the

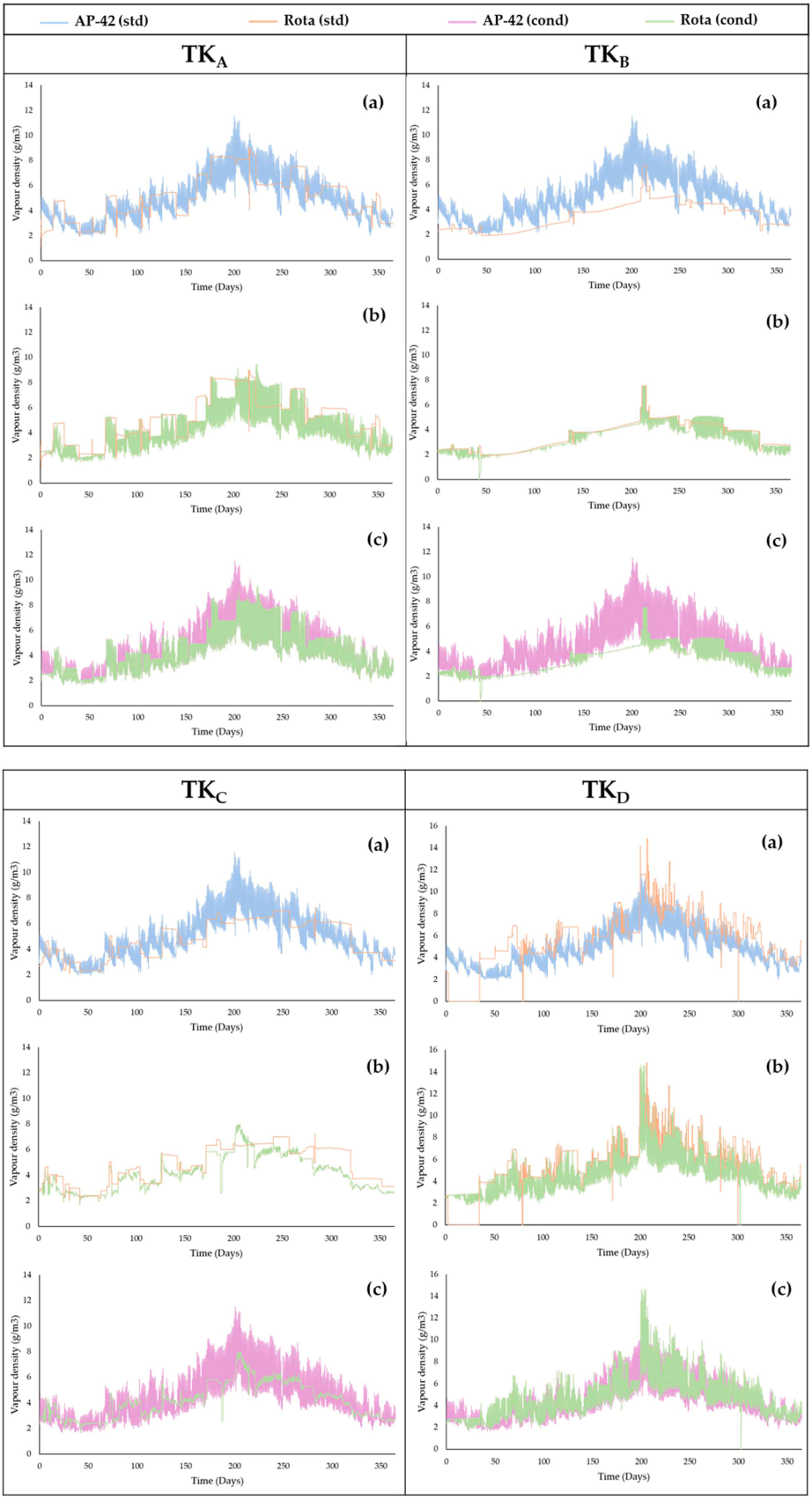

Fig. 5. Vapor density comparison for the four tanks.

corresponding outward vented vapor volume.

The vent volumetric flow rate was derived from hourly liquid-level measurements recorded by the refinery DCS. Under filling conditions, any increase in liquid volume results in an equivalent displacement of vapor from the headspace, as the tanks operate close to atmospheric pressure and the liquid phase can be considered incompressible under these conditions. The vapor volume displaced during each hourly level increment represent an outward vent flow contributing to emissions. During emptying phases, when the liquid level decreases, the headspace volume increases and ambient air is drawn into the tank rather than expelled. Consequently, no movement-induced vapor outflow is generated during these periods, and no corresponding emission mass is attributed to level decrease events. This approach is followed by both U.S. Environmental Protection Agency (2020) and Rota et al. (2001).

Table 2 reports the total annual VOC emissions (in tons/year) calculated with the different models.

All four time-series exhibit a clear seasonal modulation driven by ambient temperature, with higher concentrations in warmer months and lower values in colder periods. Crucially, the contrast between TK_B and TK_D is pronounced primarily in the Rota et al. (2001) outputs, because U.S. EPA's AP-42 Chapter 7 (U.S. Environmental Protection Agency, 2020) does not include the instantaneous tank level as a state variable and therefore responds mainly to temperature. TK_B's long, gradual filling/emptying ramps yield smooth Rota et al. 2001 time series with gentle rises and decays, whereas TK_D's operation near ~10 m with continuous micro-adjustments produces high-frequency oscillations in the Rota et al. (2001) predictions. By comparison, the AP-42 series for TK_B and TK_D remain broadly alike apart from the common seasonal envelope, reflecting their level-insensitive formulation. TK_A and TK_C show intermediate behavior, alternating more active and quiescent phases that translate into moderate temporal variability across all models.

Across methods, Rota et al. (2001) (standard and with condensation) generally predicts lower emissions than U.S. EPA's AP-42 (U.S. Environmental Protection Agency, 2020) (standard and with condensation), as confirmed by the annual totals; on an annual basis, the condensation correction changes AP-42 by approximately 11 % and Rota et al. 2001 by about 14 % on average across the four tanks, while comparing AP-42 (standard) against Rota et al. 2001 with condensation yields a mean difference of roughly 17 %.

In terms of dynamical response, AP-42 reacts more promptly to temperature changes, whereas Rota et al. (2001), particularly in the standard form, exhibits a more inertial response; adding condensation in Rota sharpens transient peaks but shortens their duration and accelerates the return to baseline. Overall, tank-to-tank differences are dominated by the level schedule in the Rota framework but are largely suppressed in AP-42 due to its level independence; model-to-model differences, in turn, reflect this structural contrast between a temperature-driven, level-insensitive formulation and a transient-resolving, level-dependent one.

Table 2
Total annual VOC emissions (tons/year) from the tanks calculated with the different models.

Model	Emission (ton/y) TK_A	Emission (ton/y) TK_B	Emission (ton/y) TK_C	Emission (ton/y) TK_D
AP-42 (std)	1.517	0.235	2.901	0.333
AP-42 (cond)	1.330	0.208	2.617	0.296
Rota (std)	1.422	0.187	2.829	0.396
Rota (cond)	1.248	0.168	2.416	0.321

4. Critical discussion

The phenomenological model of Rota et al. (2001) provides a detailed description of heat- and mass-transfer phenomena in the headspace of hydrocarbon storage tanks, though it is sensitive to the choice of initial conditions. In this study, linear vertical profiles of temperature and concentration bounded by the prescribed boundary conditions were adopted; while this assumption is reasonable in the absence of direct measurements, it introduces a degree of arbitrariness that should be considered when interpreting the results.

4.1. Role of condensation

Neglecting condensation can lead to non-physical supersaturation at the vent and to overestimation of emissions. Including a condensation treatment stabilizes the numerics and yields thermodynamically consistent emission patterns, especially under steep thermal gradients.

4.2. Sensitivity to level jitter and finite relaxation (TK_D case)

A distinctive feature of the results is the annual inversion observed for TK_D, where Rota et al. (2001) predicts higher emissions than U.S. EPA's AP-42 (U.S. Environmental Protection Agency, 2020), unlike the other tanks. TK_D is operated near a quasi-constant level (~10 m) but with continuous micro-adjustments; this "level jitter" imposes a high frequency forcing on the headspace. In Rota et al. (2001), the gas phase evolves through coupled mass- and energy-balance equations with finite relaxation times, and the level explicitly enters the boundary conditions and control volumes. Frequent small perturbations prevent full relaxation between successive disturbances, so the model resolves many short, partially dissipated transients; when integrated over the year, the cumulative area under these numerous narrow excursions can exceed that of the smoother AP-42 trajectories, yielding higher annual totals for TK_D. By contrast, U.S. EPA's AP-42 (U.S. Environmental Protection Agency, 2020) is intrinsically independent of the instantaneous level path and responds primarily to temperature (and prescribed throughput proxies), so high-frequency level oscillations do not translate into commensurate fluctuations in AP-42 emissions. The divergence between the two modeling approaches is therefore most evident under persistent level jitter and finite system relaxation, consistent with the TK_B–TK_D contrast being pronounced in Rota et al. (2001) and comparatively attenuated in U.S. EPA's AP-42 (U.S. Environmental Protection Agency, 2020).

4.3. Sensitivity to the vapour-pressure correlation

Since a single correlation determines the saturation pressure P_{VA} (and thus W_v), its uncertainty was assessed by directly comparing two diesel-specific formulations:

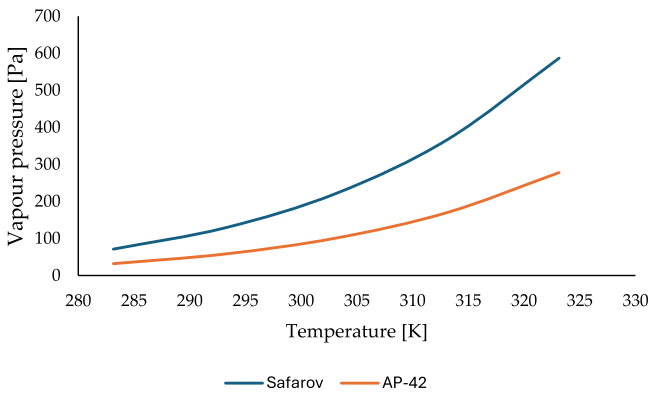

Fig. 6. Vapor pressure models comparison.

1. Safarov et al. (2019) - Diesel B0, Antoine form
2. AP-42 Chapter 7 (U.S. Environmental Protection Agency, 2020) - No. 2 Fuel Oil/Diesel, Eq. 1–25

Over 283–323 K, this comparison yielded systematic differences of about 53–55 %. These discrepancies propagate proportionally from P_{VA} to W_V and, for both U.S. EPA's AP-42 (U.S. Environmental Protection Agency, 2020) and Rota et al. (2001), to standing and working losses. Any inventory or compliance assessment should therefore either employ a correlation calibrated to the actual stored product or report uncertainty bands derived from the progression from the saturation pressure to W_V and ultimately to emissions (Fig. 6).

5. Conclusions

The objective of this study was to implement the phenomenological tank-headspace model of Rota et al. (2001) and to benchmark its performance against U.S. EPA's AP-42 (U.S. Environmental Protection Agency, 2020) in a real refinery context. The analysis focused on four fixed-roof diesel tanks monitored over a full year, with hourly records of fill level, bulk-liquid temperature, and ambient temperature. The computational framework (MATLAB 2024a) was adapted to the site-specific conditions, introducing flux limiters to handle steep gradients and a simplified condensation treatment at the roof. Model outputs were then evaluated in terms of roof-vent concentrations and the corresponding emissions, including annual totals.

In synthesis, both approaches reproduce the seasonal temperature modulation of emissions. Differences among tanks are governed largely by the level schedule, which appears explicitly in Rota et al. (2001) but not in U.S. EPA's AP-42 (U.S. Environmental Protection Agency, 2020). As a result, tank-to-tank contrasts are more pronounced in the Rota et al. 2001 outputs, whereas AP-42 time series remain primarily temperature-driven. Annual emission totals are broadly comparable across methods, with Rota et al. (2001) generally yielding lower values than U.S. EPA's AP-42 (U.S. Environmental Protection Agency, 2020), albeit with tank-specific exceptions.

With respect to the stated objectives, the Rota et al. (2001) model offers clear advantages for event-scale analysis: it resolves filling/emptying transients and headspace dynamics within a single physical framework and, once condensation is included, avoids non-physical supersaturation and yields thermodynamically consistent post-event relaxation. This transient-resolving capability makes it particularly suited to short-term exposure assessment, operational scheduling, and the diagnostic analysis of peak-driven episodes.

On the other hand, important limitations emerged for inventory-type objectives. The model exhibits slow adaptability to operating changes—particularly in the version without condensation—responding more sluggishly to temperature and level fluctuations than observed in plant data. Benchmarks were run on the computational setup described in Section 2.3. On this system, a full-year simulation requires approximately 10 min per tank; at refinery scale—potentially involving hundreds of tanks— this translates into several thousand minutes of wall-clock time, whereas the U.S. EPA's AP-42 workflow is effectively instantaneous in a spreadsheet. Given that annual emission totals differ only modestly between methods, the cost–benefit of the transient-resolving solver for regulatory inventories appears limited; its added value is clearest at high temporal resolution, not in yearly aggregates. Moreover, the phenomenological approach places greater demands on inputs (initial and boundary profiles, thermal characterization, and vapour-pressure correlation choice), which can introduce additional uncertainty if site-specific data are scarce.

Overall, with respect to the objectives defined at the outset, the model of Rota et al. (2001) proves most effective when the problem requires a mechanistic, transient-resolving view of emissions and peak behavior, while U.S. EPA's AP-42 (U.S. Environmental Protection Agency, 2020) remains a pragmatic and proportionate tool for annual inventory development, given its simplicity, speed, and the modest differences observed in yearly totals.

Future work should prioritise improved thermal characterisation of T_B, T_{AA}, and especially T_t, which largely governs T_V and phase equilibrium, together with field measurements of headspace concentrations to reduce dependence on assumed initial profiles. In addition, given the demonstrated sensitivity of emission estimates to the selected vapour-pressure correlation, future developments should incorporate explicit uncertainty quantification and, where feasible, multicomponent thermodynamic representations of stored products.

Supplementary material

The codes developed for this study are freely available at the link: https://github.com/DiegoRampi/TANK-emission-code/tree/main.

CRediT authorship contribution statement

Diego Rampi: Writing – original draft, Visualization, Software, Methodology, Investigation, Data curation. **Francesca Tagliaferri:** Writing – review & editing, Supervision, Methodology, Investigation, Data curation, Conceptualization. **Marzio Invernizzi:** Writing – review & editing, Supervision, Methodology, Investigation, Data curation, Conceptualization.

Declaration of competing interest

The authors declare that they have no known competing financial interests or personal relationships that could have appeared to influence the work reported in this paper.

Data availability

Research Link Provided
Numerical model implementation and simulation code for VOC tank emission modeling (Original data) (GitHub)

References

Atkinson, R., 1990. Gas-phase tropospheric chemistry of organic compounds: a review. Atmos. Environ.
Batić, I.M., 2023. Reduction of evaporation losses in oil and oil derivatives storage tanks: a case study for warehouse in Požega, Serbia. Therm. Sci. 27, 2455–2464. https://doi.org/10.2298/TSCI220923172B.
Bo, Y., Cai, H., Xie, S.D., 2008. Spatial and temporal variation of emission inventories for historical anthropogenic NMVOCs in China. Atmosph. Chem. Phys. Discuss. 8, 11519–11566. https://doi.org/10.5194/acpd-8-11519-2008.
Butt, J.B., 2000. Reaction-Kinetics-and-Reactor-Design-2nd-edition.
Chen, D., Xu, Y., Xu, J., Lian, M., Zhang, W., Wu, W., Wu, M., Zhao, J., 2022. The vertical distribution of VOCs and their impact on the environment: a review. Atmosphere. https://doi.org/10.3390/atmos13121940.
Dicke, M., Baldwin, I.T., 2010. The evolutionary context for herbivore-induced plant volatiles: beyond the "cry for help". Trends. Plant Sci. https://doi.org/10.1016/j.tplants.2009.12.002.
Dicke, M., Loreto, F., Manager, J., Kastelein, J., Administrator, J., Rietveld, M., Christensen, N.M., Oparka, K.J., Tilsner, J., Mosher, R.A., Melnyk, C.W., Pruneda-Paz, J.L., Kay, S.A., Peñuelas, J., Staudt, M., Niinemets, Ü., Schnitzler, J.-P., Baldwin, I.T., Holopainen, J.K., Gershenzon, J., Arneth, A., Kegge, W., Pierik, R., 2010. Forthcoming articles advances in imaging RNA in plants siRNA and DNA methylation: seedy epigenetics an expanding universe of circadian networks in higher plants special issue: induced biogenic volatile organic compounds from plants 115 induced plant volatiles: from genes to climate change.
Duan, C., Liao, H., Wang, K., Ren, Y., 2023. The research hotspots and trends of volatile organic compound emissions from anthropogenic and natural sources: a systematic quantitative review. Environ. Res. https://doi.org/10.1016/j.envres.2022.114386.
Elliott~, R.W., Watts, H., n.d. Diffusion of some hydrocarbons in air: a regularity in the Diffusion coefficients of a homologous Series1.
Fetisov, V., Gonopolsky, A.M., Davardoost, H., Ghanbari, A.R., Mohammadi, A.H., 2023. Regulation and impact of VOC and CO2 emissions on low-carbon energy systems resilient to climate change: a case study on an environmental issue in the oil and gas industry. Energy Sci. Eng. https://doi.org/10.1002/ese3.1383.

Guenther, A., 1997. Seasonal and spatial variations in natural volatile organic compound emissions. Ecol. Appl. https://doi.org/10.1890/1051-0761(1997)007[0034:SASVIN]2.0.CO;2.
Holopainen, J.K., Gershenzon, J., 2010. Multiple stress factors and the emission of plant VOCs. Trends Plant Sci. https://doi.org/10.1016/j.tplants.2010.01.006.
Invernizzi, M., Roveda, L., Polvara, E., Sironi, S., 2021. Lights and shadows of the voc emission quantification. Chem. Eng. Trans. 85, 109–114. https://doi.org/10.3303/CET2185019.
Invernizzi, M., Sironi, S., 2021. Odour emission rate estimation methods for hydrocarbon storage tanks. Chem. Eng. Trans. 85, 67–72. https://doi.org/10.3303/CET2185012.
Invernizzi, M., Tagliaferri, F., Manganelli, C., Sironi, S., 2025. Quantitative estimation of odorous emissions from heterogeneous area sources via thermal imaging drone. Sci. Total Environ. 1000. https://doi.org/10.1016/j.scitotenv.2025.180415.
Kansal, A., 2009. Sources and reactivity of NMHCs and VOCs in the atmosphere: a review. J. Hazard. Mater. 166, 17–26. https://doi.org/10.1016/j.jhazmat.2008.11.048.
Kegge, W., Pierik, R., 2010. Biogenic volatile organic compounds and plant competition. Trends. Plant Sci. 15, 126–132. https://doi.org/10.1016/j.tplants.2009.11.007.
LeVeque, R.J., 1990. Numerical Methods for Conservation Laws.
Liaskoni, M., Huszár, P., Bartík, L., Perez, A.P.P., Karlický, J., Šindelářová, K., 2024. The long-term impact of biogenic volatile organic compound emissions on urban ozone patterns over central Europe: contributions from urban and rural vegetation. Atmos. Chem. Phys. 24, 13541–13569. https://doi.org/10.5194/acp-24-13541-2024.
Majumdar, A., LeClair, A., Hartwig, J., Ghiaasiaan, S.M., 2023. Numerical modeling of no vent filling of a cryogenic tank with thermodynamic vent system augmented injector. Cryogenics 131. https://doi.org/10.1016/j.cryogenics.2023.103651.
Mellouki, A., Wallington, T.J., Chen, J., 2015. Atmospheric chemistry of oxygenated volatile organic compounds: impacts on air quality and climate. Chem. Rev. https://doi.org/10.1021/cr500549n.
Moncalvo, D., Davies, M., Weber, R., Scholz, R., 2016. Breathing losses from low-pressure storage tanks due to atmospheric weather change. J. Loss. Prev. Process. Ind. 43, 702–705. https://doi.org/10.1016/j.jlp.2016.06.006.
Niinemets, Ü., 2010. Mild versus severe stress and BVOCs: thresholds, priming and consequences. Trends Plant Sci. https://doi.org/10.1016/j.tplants.2009.11.008.
Pandey, P., Yadav, R., 2018. A review on volatile organic compounds (VOCs) as environmental pollutants: fate and distribution. Int. J. Plant Environ. 4, 14–26. https://doi.org/10.18811/ijpen.v4i02.2.
Pascal, B., Chaugny, M., Sancho, Luis.D., Roudier, S., 2015. Best available techniques (BAT) reference document for the refining of mineral oil and gas industrial emissions: industrial Emissions Directive 2010/75/EU (integrated pollution prevention and control). Publications Office. https://doi.org/10.2791/01075.
Piccot, S.D., Watson, J.J., Jones, J.W., 1992. A global inventory of volatile organic compound emissions from anthropogenic sources. J. Geophys. Res.
Polvara, E., Roveda, L., Invernizzi, M., Capelli, L., Sironi, S., 2021. Estimation of emission factors for hazardous air pollutants from petroleum refineries. Atmosphere 12. https://doi.org/10.3390/atmos12111531.
Ra, Y., Reitz, R.D., McFarlane, J., Daw, C.S., 2009. Effects of fuel physical properties on diesel engine combustion using diesel and bio-diesel fuels. SAE Int. J. Fuels. Lubr. 1, 703–718. https://doi.org/10.4271/2008-01-1379.
Rota, R., Frattini, S., Astori, S., Paludetto, R., 2001. Emissions from fixed-roof storage tanks: modeling and experiments. Ind. Eng. Chem. Res. 40, 5847–5857. https://doi.org/10.1021/ie010111m.
Safarov, J., Ashurova, U., Ahmadov, B., Hassel, E., 2019. Vapour pressure of 1-butanol and diesel B0 binary fuel blends. J. Serb. Chem. Soc. 84, 599–607. https://doi.org/10.2298/JSC180521015S.
Saikomol, S., Thepanondh, S., Laowagul, W., 2019. Emission losses and dispersion of volatile organic compounds from tank farm of petroleum refinery complex. J. Environ. Health Sci. Eng. 17, 561–570. https://doi.org/10.1007/s40201-019-00370-1.
Soni, V., Singh, P., Shree, V., Goel, V., 2018. Effects of VOCs on human health. Energy, Environment, and Sustainability. Springer Nature, pp. 119–142. https://doi.org/10.1007/978-981-10-7185-0_8.
Sun, S., Palmer, P.I., Siddans, R., Kerridge, B.J., Ventress, L., Edtbauer, A., Ringsdorf, A., Pfannerstill, E.Y., Williams, J., 2025. Seasonal isoprene emission estimates over tropical South America inferred from satellite observations of isoprene. https://doi.org/10.5194/egusphere-2025-778.
Sweby, P.K., 1984. High resolution schemes using flux limiters for hyperbolic conservation laws. SIAM J. Numer. Anal.
Tagliaferri, F., Invernizzi, M., Sironi, S., 2023. Experimental evaluation on liquid area sources: influence of wind velocity and temperature on the wind tunnel sampling of VOCs emissions from wastewater treatment plants. Chemosphere 312, 137337. https://doi.org/10.1016/j.chemosphere.2022.137337.
Tagliaferri, F., Sironi, S., Invernizzi, M., 2026. Assessing VOC dispersion from hydrocarbon storage tanks: a case study on emission temporal resolution. Appl. Sci. 16 (4), 1851. https://doi.org/10.3390/app16041851.
U.S. Environmental Protection Agency, 2020. AP-42, Compilation of Air Pollutant Emission Factors: Chapter 7 – Liquid Storage Tanks.
Wang, H.L., Nie, L., Li, J., Wang, Y.F., Wang, G., Wang, J.H., Hao, Z.P., 2013. Characterization and assessment of volatile organic compounds (VOCs) emissions from typical industries. Chin. Sci. Bull. 58, 724–730. https://doi.org/10.1007/s11434-012-5345-2.
Wang, Y., Liu, M., Liu, F., Zhao, C., Zhao, D., Han, F., Liu, C., 2018. Research on the effect of wall corrosion and rim seal on the withdrawal loss for a floating roof tank. Environ. Sci. Pollut. Res. 25, 18434–18442. https://doi.org/10.1007/s11356-018-1978-2.
Wei, W., Chen, S., Wang, Y., Cheng, L., Wang, X., Cheng, S., 2022. The impacts of VOCs on PM2.5 increasing via their chemical losses estimates: a case study in a typical industrial city of China. Atmos. Environ. 273. https://doi.org/10.1016/j.atmosenv.2022.118978.
Xing, C., Liu, C., Lin, J., Tan, W., Liu, T., 2024. VOCs hyperspectral imaging: a new insight into evaluate emissions and the corresponding health risk from industries. J. Hazard. Mater. 461. https://doi.org/10.1016/j.jhazmat.2023.132573.
Zhou, L., Jiao, X., Yang, B., Yuan, W., Zhao, W., Zhang, L., Huang, W., Long, S., Xu, J., Shen, H., Wang, C., 2025. The impact of indoor environments on the abundance of urban outdoor VOCs. Environ. Sci. Technol. https://doi.org/10.1021/acs.est.4c13133.
Zhou, X., Zhou, X., Wang, C., Zhou, H., 2023. Environmental and human health impacts of volatile organic compounds: a perspective review. Chemosphere 313. https://doi.org/10.1016/j.chemosphere.2022.137489.
Zinke, R., Melnychuk, J., Köhler, F., Krause, U., 2020. Quantitative risk assessment of emissions from external floating roof tanks during normal operation and in case of damages using Bayesian Networks. Reliab. Eng. Syst. Saf. 197, 106826. https://doi.org/10.1016/j.ress.2020.106826.